A New Vehicle Specific Power Model for the Estimation of Hybrid Vehicle Emissions

Ante Kozina , Tino Vidović , Gojmir Radica * , Ante Vučetić

Posted Date: 9 November 2023

doi: 10.20944/preprints202311.0600.v1

Keywords: Hybrid Electric Vehicles; Vehicles models; VSP analyses

Article

A new Vehicle Specific Power Model for the Estimation of Hybrid Vehicle Emissions

Ante Kozina [1], Tino Vidović [1], Gojmir Radica [1,*] and Ante Vučetić [2]

[1] University of Split, Faculty of Electrical Engineering, Mechanical Engineering and Naval Architecture, R. Boškovića 32, 21000 Split, Croatia
[2] University of Zagreb, Faculty of Mechanical Engineering and Naval Architecture, Ivana Lučića 5 10000 Zagreb, Croatia
* Correspondence: goradica@fesb.hr

Abstract: Hybrid electric vehicles are certainly one of the key solutions for improving fuel efficiency and reducing emissions, especially in special vehicle application and with the use of CO_2 neutral fuels. Determining the energy management strategy and finding the optimal solution with regard to the aforementioned goals remains the one of the main challenges in the design of HEV. This paper presents a new vehicle modeling method, with an emphasis on HEVs, which is based on the frequency analysis of emissions and consumption according to the current specific traction power of the vehicle. The evaluation of the newly introduced model in the RDE, NEDC and WLTP cycle was performed and the results were compared with the standard verified vehicle model that was created in AVL's CruiseM software package. Positive traction energies have positive deviations of between 0.35% and 2.85%. The largest deviation in CO_2 emissions was recorded for the HEV model in the RDE cycle and in the non-hybrid model in the WLTP cycle of 3.79% and 4.4% respectively, all other combinations of cycle and vehicles had deviations of up to about 1%. As expected, the largest relative deviations were recorded for NOx emissions from 0.13% to 9.62% for HEV in the WLTP cycle.

Keywords: Hybrid Electric Vehicles; Vehicles models; VSP analyses

1. Introduction

The constant increase in transport needs and the desire for sustainability is forcing vehicle manufacturers towards significant reductions in harmful exhaust emissions and emissions of greenhouse gases, especially carbon dioxide. Several countries, especially EU members and some US states, are planning to ban the sale of new passenger vehicles powered by fossil fuels [1], but this prohibition model has been difficult to apply in the less developed parts of the world with underdeveloped infrastructure [2]. The EU plans to reduce CO_2 emissions to 95g/km for new passenger vehicles by 2025 [3], an additional reduction of 17% is planned between 2025 and 2030, and a reduction of 37.5% from 2030 onwards [4]. In the last 15 years, high-speed internal combustion engines have achieved very high efficiency, diesel engines achieve peak mechanical efficiency of over 40% [5], but still can barely meet the requirements of the next Euro 7 standard as a stand-alone powertrain [6]. The main reason for this is the inefficient energy management due to absence of regenerative braking and a large drop in efficiency at low loads due to engine operation at low efficiency region. Hybrid Electric Vehicles (HEVs) combine the advantages of EVs and standard vehicles, they have a high degree of flexibility as well as the ability to meet a wider range of driving requirements [7]. The most significant advantage compared to standard vehicles powered only by an ICE is a far more efficient disposal of mechanical energy through the possibility of saving energy from regenerative braking or storing excess energy when moving the engine operating region towards the one with the highest efficiency of the internal combustion engine, as well as the use of smaller, lighter and simpler single-range ICE. Also, the constant possibility of choosing different operating parameters of the ICE enables a better emission control management and almost completely solves their problems in exploitation [8]. The most significant advantage of HEVs compared to fully electric vehicles (EVs) is their superior range with a single charge and fast refueling,

 doi:10.20944/preprints202311.0600.v1

which is achieved by using chemical energy instead of electricity [9]. Hybrid electric vehicles are one of the key solutions for increasing efficiency and reducing emissions, especially with the use of environmentally friendly, synthetic CO_2 neutral fuels at an acceptable price [10] or for developing countries alternative fuels such as LPG with significantly lower emissions and CO_2 footprint [11]. Such power trains will certainly find their application in heavy trucks for long distances, special purpose vehicles, off road and military vehicles [12,13]. The share of hybrid vehicles, with all levels of hybridization from plug-in hybrid electric vehicles, full hybrid vehicles, to mild hybrid vehicles, predicts to be over 36% by 2030 [14]. The above indicated advantages are made possible due to the high complexity of the HEV system, which is also the biggest challenge both in terms of the number of installed systems and in terms of finding the optimal control method [15–17]. The use of multiple energy sources and the high complexity of the HEV drive system require a more complex high-level control system that in turn requires complex modeling methods with high demanding models in user and computational terms [18–20]. Various approaches to the modeling of hybrid road vehicles have been developed and, according to literature, we distinguish kinematic (backward approach), quasi-static (forward approach) and dynamic models [21,22]. The optimal solution depends on the specifics of the application, but in most cases the energy management strategy is a compromise between minimizing energy consumption and exhaust gas emissions [23], increasing the durability of components such as batteries, meeting power requirements, ensuring vehicle performance and comfort [24].

The main goal of this paper is to present a new Vehicle Specific Power (VSP) model of a hybrid vehicle based on frequency analysis of energy, emissions and consumption. This method should enable a faster and easier arrival at the pre-set HEV optimization objective, or it can be used as a guideline that leads to an optimal solution avoiding local minima. The model is based on a real vehicle emissions, fuel and energy consumption which were recorded in real driving conditions according to the Real Driving Emissions (RDE) rules which are today mandatory segment of type approval process. Validation and result comparison was done regarding to standard time based CruiseM model results.

2. Materials and Methods

First a non-hybrid vehicle model was created and validated in AVL's CruiseM software package. The purpose of this model is to check the accuracy of the newly introduced VSP frequency model in different tested conditions or cycles. A new VSP model was developed based on the specific power of the vehicle, and frequency analysis. The CruiseM model is based on maps of consumption and emissions which were obtained with chassis dynamometer in laboratory conditions. The vehicle models are validated with obtained parameters under RDE driving cycle. Next step was hybridization of both models into a parallel hybrid electric vehicle under equal conditions with CruiseM model as a control model. At the end, the obtained results of the newly developed VSP frequency model and the time domain CruiseM model were compared. The comparison was made on a non-hybrid and hybrid vehicle in RDE, NEDC and WLTC cycles.

2.1. Measurement and Equipment

Portable emissions measurement system (PEMS) AVL M.O.V.E. was installed on a test vehicle for the purpose of measuring emissions carbon dioxide and other pollutants in real driving conditions. This system continuously monitors and records data vehicle emissions. The PEMS device is composed of several basic parts that are interconnected and controlled by a central computer. More detailed information about the AVL M.O.V.E. measuring instrument is shown in the Figure 1.

Preprints (www.preprints.org) | NOT PEER-REVIEWED | Posted: 9 November 2023 doi:10.20944/preprints202311.0600.v1

Analyzer	NO/NO_2 and $CO/CO_2/N_2O$	THC/CH_4	Particle counter
Measuring method	Non-Dispersive Ultra Violet – NDUV Non-Dispersive Infrared – NDIR	Flame Ionisation Detector – FID	Advanced diffusion charger
Measuring range	NO: 0 do 5000 ppm	THC: 0 do 30000 ppmC1	from ~1500 to ~2,5 x 107 #/cm^3
	NO_2: 0 do 2500 ppm		
	CO: 0 do 5% vol.		
	CO_2: 0 do 20% vol.	CH_4: 0 do 10000 ppmC1	
	N_2O: 0 do 2000 ppm		
Zero drift/8h	NO/NO_2: 2 ppm	± 5 ppm C1/8h	
	CO: 20 ppm		
	CO_2: 0,1% vol.		
	N_2O: 20 ppm		
Accuracy		0,3% FS	

Figure 1. Technical features of PEMS devices.

To diminish impact on the driving dynamics the majority of equipment is installed in the trunk of the vehicle: gas analysers, solid particle counter, central computer and battery Exhaust gas mass flow meter, GPS receiver and meteorological station for monitoring atmospheric conditions are installed outside. Photo of the vehicle with all the measuring equipment is shown in Figure 2. Measurements of current power, consumption and emissions were recorded on a 87 km long route that meets the RDE measurement criteria and all measurements were performed according to the RDE test procedure. The calibration of the measuring instruments was performed before the start of the measurement and after the measurement was completed. Continuous power measurement was carried out via OBD diagnostics, whose power values were previously calibrated on chassis dynamometer at several operating points throughout the entire engine operating range. The emission maps and consumption maps that were used in the creation of the time domain CruiseM model were obtained by measuring emissions and consumption on chassis test bed at different engine loads and speeds. In all laboratory measurements, a MAHA chassis dynamometer LPS 3000 was used. The vehicle was type approved according to the EURO6b standard based on the laboratory NEDC test cycle, which characteristics are shown in Table 1. Coast-down analysis was used to determine the resistances of the vehicle. This was obtained by recording the speed from the OBD system with a resolution of 1s. The measured speed from OBD was previously calibrated with the GPS system.

Table 1. Characteristics of the tested vehicle.

Year of Production	Emission Norm	Engine Volume l	Max. Power kW/HP	Max. Engine Torque Nm	Anti pollution Systems	Fuel	Transmission	Weight kg
2014	Euro 6	1.6	77/105	250	EGR, DOC, DPF	Diesel	Manual 5s	1395

Figure 2. Test vehicle with built-in measuring equipment.

Preprints (www.preprints.org) | NOT PEER-REVIEWED | Posted: 9 November 2023 doi:10.20944/preprints202311.0600.v1

The vehicle model was created in the CruiseM software package with a quasi-static or forward approach, which starts from the driver's request to follow predetermined speed pattern or driving cycle, schematic representation is on Figure 3. The request is transmitted to the drive system via the appropriate regulator and accelerator pedal which has its own characteristics and transient response. The torque is transmitted to the transmission system, which has its own gear ratios and losses all the way to the wheels, which needs to achieve the necessary torque or driving force to meet the required velocity pattern. This approach gives particularly good results in CO_2 emissions, consumption estimation as well as NOx emissions estimation [21].

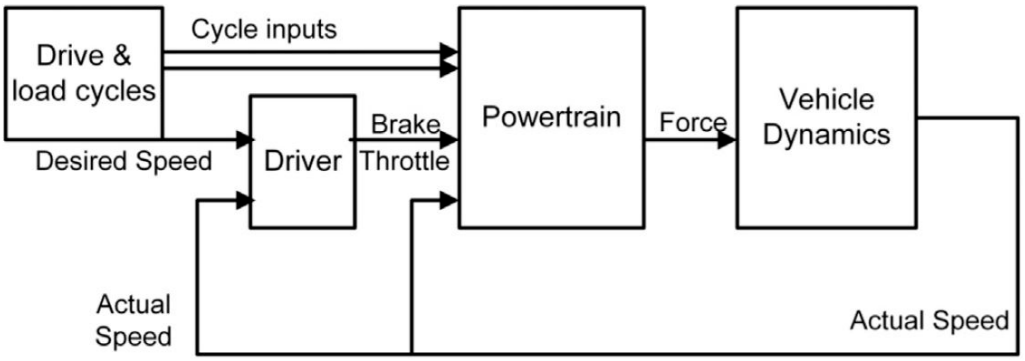

Figure 3. Schematic representation of the quasi-static or Forward model of the vehicle [21].

A full hybrid vehicle with a parallel configuration was modelled. The same model was also used in the simulation of a non-hybrid vehicle with the exclusion of the corresponding components, marked blue in Figure 4. As it is a moderate daily driving style, the transverse and vertical dynamics have negligible influence, so the model was reduced to longitudinal vehicle dynamics described by a physical model. The vehicle resistance forces are defined as a function of the vehicle speed, by a polynomial of second degree (1) obtained from the Coast Down analysis [25]. Vehicle drag force equation is defined as:

$$f_0 + f_1 \times v + f_2 \times v^2 = TM \frac{dv}{dt} \quad (1)$$

where parameter f0 is the free term, f1 is the linear component and f2 is the quadratic component.

The internal combustion engine is modeled as a black box based on the corresponding consumption or CO_2 maps, and NOx maps which give the correlation of the corresponding emissions with the engine current operating point. Engine maps were also obtained by testing on chassis test bed sweeping the entire operating range. Engine is controlled by desired load from controller. Engine limits are determined by the maximum torque as a function of rotation speed. The motoring torque losses were set up with interpolation curve depending on the speed of rotation. A classic gearbox with 5 forward gears is modeled, with the same transmission ratios as the physical one. The efficiency as well as the moments of inertia were held constant. The vehicle powertrain contains two clutches, the first one (separator) serves to separate the ICE from the rest of the Powertrain and the second one is a standard clutch for coupling power devices with the transmission. The separator enables to connect/disconnect the ICE to/from the whole system according to the applied HEV strategy (e.g., e-drive, e-brake regeneration, etc.). In addition, a transmission controller is required for gear up-/downshifting as well as actuating both clutches. Both clutches are driven by thrust force and modeled with following parameters: maximum torque, moment of inertia and "clutch release" dependence characteristic on thrust force.

A 48V electric drive system was used, which consists of a battery, a power consumer and an electric machine (EM) that is mechanically connected between two clutches. The EM is modeled as a basic quasi-static model that instantly responds to the torque demand. The characteristics of EM are defined in both working quadrants separately. The maximum torque limit is defined in generator

Preprints (www.preprints.org) | NOT PEER-REVIEWED | Posted: 9 November 2023 doi:10.20944/preprints202311.0600.v1

and motor mode depending on the rotation speed as well as the efficiency characteristics with an additional parameter of the operating voltage. The drive control calculates the e-motor load signal in both traction and recuperation conditions, by modifying the cockpit output signals. If the braking effect of the e-motor torque is below the driver's request in terms of equivalent brake pressure, then the mechanical brakes are supplied with pressure. The HEV controller contains a basic state machine which smoothly applies different hybrid strategies according to the current driving situation. A baseline management strategy was chosen according to the rules, which does not have the ability to adapt to different driving conditions [26], so that the change of control parameters during testing in different cycles was done manually. For an easier comparison of fuel and energy consumption between different models, the Charge Sustain mode was used, which requires the battery to be equally charged at the beginning and at the end of the each testing cycle.

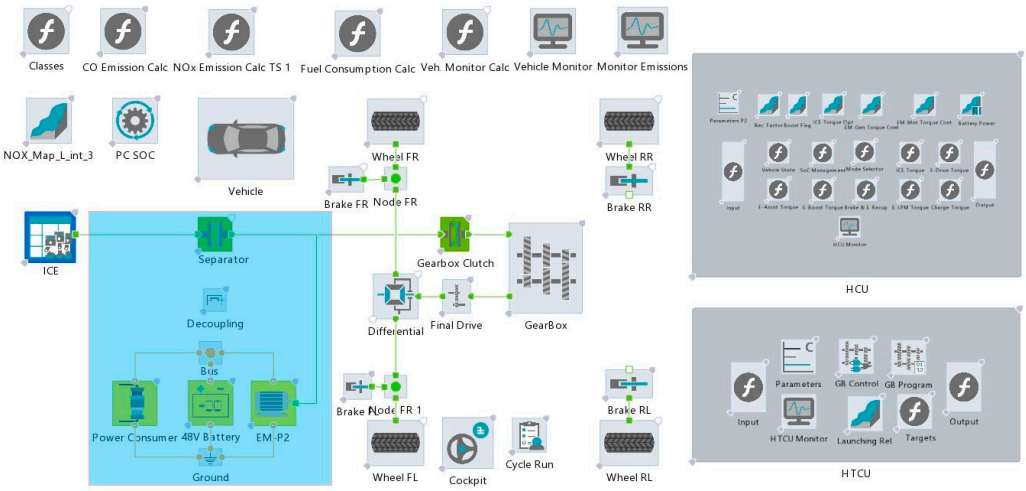

Figure 4. Schematic representation of the CruiseM vehicle model.

2.2. VSP Model

Vehicle specific power (VSP) is defined as a ratio of the instantaneous power to the vehicle's mass, which is used on overcoming the vehicle's resistances, which includes rolling and aerodynamic resistances, and kinetic and potential energies (2) [27]:

$$VSP = \frac{\frac{d}{dt}(KE + PE) + F_{roll} \cdot v + F_{aero} \cdot v}{m} = \frac{\frac{d}{dt}(KE + PE) + F_{res} \cdot v}{m} = \frac{\frac{d}{dt}\left(\frac{1}{2}m \cdot v^2 + mgh\right) + (f_0 + f_1 \times v + f_2 \times v^2) \cdot v}{m} \quad (2)$$

All vehicle resistances including rolling resistances are also defined by longitudinal dynamics as in the classic Cruise M model with the fact that moments of inertia are approximated with a 3% increase in vehicle mass [28]. The total traction energy is calculated according to:

$$E_{tr} = \int_0^T mVSPdt \quad (3)$$

The mathematical description of the vehicle's specific power (2) is the basis for the model of the current traction power or energy consumption. This model was created using a kinematic or backward approach that starts from the end components of the vehicle, i.e. the wheels, which require a certain torque to follow the cycle. The schematic representation of the backward model is shown in Figure 5, the flow of information or requests is opposite to the flow of energy. The movement of the vehicle absolutely coincides with the cycle being followed, so additional condition is added which takes into account whether vehicle can meet power request in every point of the driving cycle.

Preprints (www.preprints.org) | NOT PEER-REVIEWED | Posted: 9 November 2023 doi:10.20944/preprints202311.0600.v1

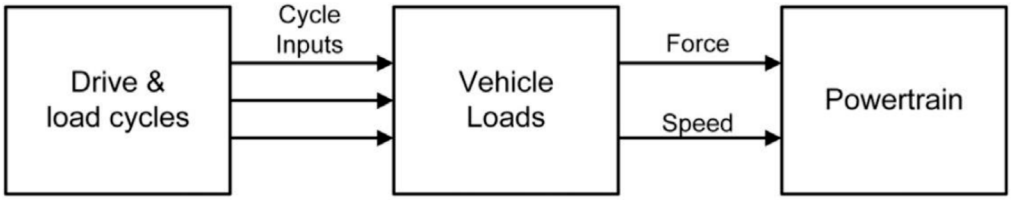

Figure 5. Schematic representation of the kinematic or backward model of the vehicle [21].

The VSP model is a discrete model formed by frequency analysis of measured emissions and consumption within certain power ranges or classes. The starting assumption is that the amount of each emission per unit of traction energy are always equal within the observed power class, regardless of the driving cycle. More accurate results are obtained by using a larger number of small ranges classes, but a large number of classes increases the complexity of data processing. The power classes are determined according to the power binning method within EU regulation 2016/427 [29], which gives normalized values of their power ranges. Some changes are introduced in classes 2 and 3. The change in the 2nd class refers to the division into its positive and negative parts separately, and class 3 is divided into two equal parts in order to increase the accuracy of the model. The denormalized values of power class ranges for the tested vehicle are shown in Table 2.

Table 2. Power classes for modelled vehicle.

Power class No	Pc,j [kW] from	Pc,j [kW] to
1	-∞	-2.368
2	-2.368	0.000
3	0.000	2.368
4	2.368	11.840
5	11.840	23.680
6	23.680	44.992
7	44.992	66.304
8	66.304	∞

The bin classification is done according to the limits specified in Table 2, and according to the conditions of maximum and minimum traction power according to (4):

$$P_{c,j\ lower\ bound} < \quad P_{wheel} \leq P_{c,j\ upper\ bound} \tag{4}$$

The bin classification is done according to the limits specified in Table 2, and according to the conditions of maximum and minimum traction power according to (4):

$$m_{x,j} = \sum_{all\ \boldsymbol{k}\ in\ class\ \boldsymbol{j}} m_{x,k} \tag{5}$$

The traction energy of the j class is calculated according to (6):

$$W_{tr,j} = m_{vehicle} \sum_{all\ \boldsymbol{k}\ in\ class\ \boldsymbol{j}} VSP_{tr,k} t_k \tag{6}$$

The value of individual emissions per unit of traction energy of the j class is equal to the ratio of the total amount of emissions of the grade and its total traction energy (7):

$$\dot{m}_{x,j} = \frac{m_{x,j}}{W_{tr,j}} = \frac{\sum_{all\ \boldsymbol{k}\ in\ class\ \boldsymbol{j}} m_{x,k}}{\sum_{all\ \boldsymbol{k}\ in\ class\ \boldsymbol{j}} P_{tr,k} t_k} = \frac{\sum_{all\ \boldsymbol{k}\ in\ class\ \boldsymbol{j}} m_{x,k}}{m_{vehicle} \sum_{all\ \boldsymbol{k}\ in\ class\ \boldsymbol{j}} VSP_{tr,k} t_k} \tag{7}$$

The distribution of emissions and energy by power classes during the testing in real driving conditions are shown in diagram in Figure 6. The energy shares of the classes are expressed in percentage relative to the total positive traction energy.

Preprints (www.preprints.org) | NOT PEER-REVIEWED | Posted: 9 November 2023 doi:10.20944/preprints202311.0600.v1

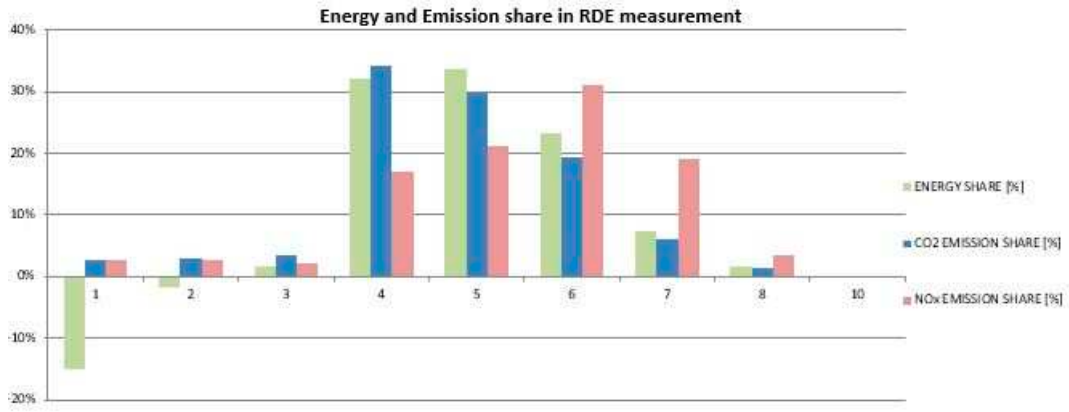

Figure 6. Classes distribution of traction energy, CO_2 emissions and NOx emissions during RDE route.

The total amount of emissions and consumption is obtained by summing the emissions of all individual classes, i.e., the product of specific emissions and the traction energy coming from the internal combustion engine, according to (8):

$$M_x = \sum_j m_{x,j} = \sum_j \dot{m}_{x,j}\, W_{tr,j} \tag{8}$$

At modelling of a non-hybrid vehicle, all power classes were calculated in the assessment of complete cycle emissions. The main point of hybrid vehicles, including this hybrid vehicle model, is to use the most favourable operation regions of each available power source, according to a defined objective function that usually evaluates emissions and consumption. Traction energy of the j- class produced by an internal combustion engine is given in (9):

$$W_{tr,j} = w_{tr,j} + w_{mwa,j} - \gamma_j w'_{stored} \tag{9}$$

$w_{tr,j}$ represents the total traction energy of j class that the engine would generate without hybrid drivetrain components, $w_{mwa,j}$ represents the additional mechanical energy due to the shift of the operating region of the engine to the more favorable class. Stored energy w'_{stored} (10) consists of the regenerative braking energy W_{br} and the stored energy of the engine produced by moving operating region $W_{s,mwa}$

$$w'_{stored} = \eta_g \eta_{st} \eta_m \left(\alpha \eta_{gb}^2 \eta_f^2 W_{br} + \eta_{gb} \eta_f W_{s,mwa}\right) \tag{10}$$

Inserting equation (10) into equation (9):

$$W_{tr,j} = w_{tr,j} + w_{mwp,j} - \gamma_j \eta_g \eta_{st} \eta_m \left(\alpha \eta_{gb}^2 \eta_f^2 W_{br} + \eta_{gb} \eta_f W_{s,mwa}\right) \tag{11}$$

The energy flows are based on the flow diagram from [30] with slightly modified labels and definition of all energy sources and sinks with regard to the drive shaft. The objective function is the minimum product of certain emissions and associated weighting factors (12):

$$\mathrm{J} = AM_{CO2} + BM_{NOx} + CM_{PN} + DM_{CO} \tag{12}$$

Due to the limitations of the classic CruiseM model, only CO_2, fuel consumption and NOx emissions, were retained, and the objective function (13) preferred only the minimization of consumption and CO_2 emissions:

$$\mathrm{J} = AM_{CO2} = \sum_j \dot{m}_{CO2,j}\, W_{tr,j} \tag{13}$$

Inserting equation (11) into (13) gives (14):

Preprints (www.preprints.org) | NOT PEER-REVIEWED | Posted: 9 November 2023 doi:10.20944/preprints202311.0600.v1

$$J = A\sum_j \dot{m}_{CO2,j}\left[w_{tr,j} + W_{mwp,j} - \gamma_j\eta_g\eta_{st}\eta_m\left(\alpha\eta_{gb}^2\eta_f^2 W_{br} - \eta_{gb}\eta_f W_{s,mwa}\right)\right] \quad (14)$$

The total stored engine moving operating region energy is obtained by multiplying power differences between the engine average *j*-class power $P_{e,j}$ and required traction power *j*-th class with engine operating time $T_{j,mwa}$ (15):

$$W_{s,mwa} = \sum_j T_{j,mwa}(P_{e,j} - P_j) \quad (15)$$

The total recuperated energy from braking is obtained by the sum of the braking energies of all individual classes (16):

$$W_{br} = \sum_j W_{br,j} \quad (15)$$

3. Results and Discussion

3.1. Vehicle Models

Based on emission measurements and other relevant parameters, a CruiseM model, as well as a new frequency model of a non-hybrid vehicle was created. The vehicle energy balance and the main conversion pathways of chemical energy derived from the fuel are shown in the diagram in Figure 7 below:

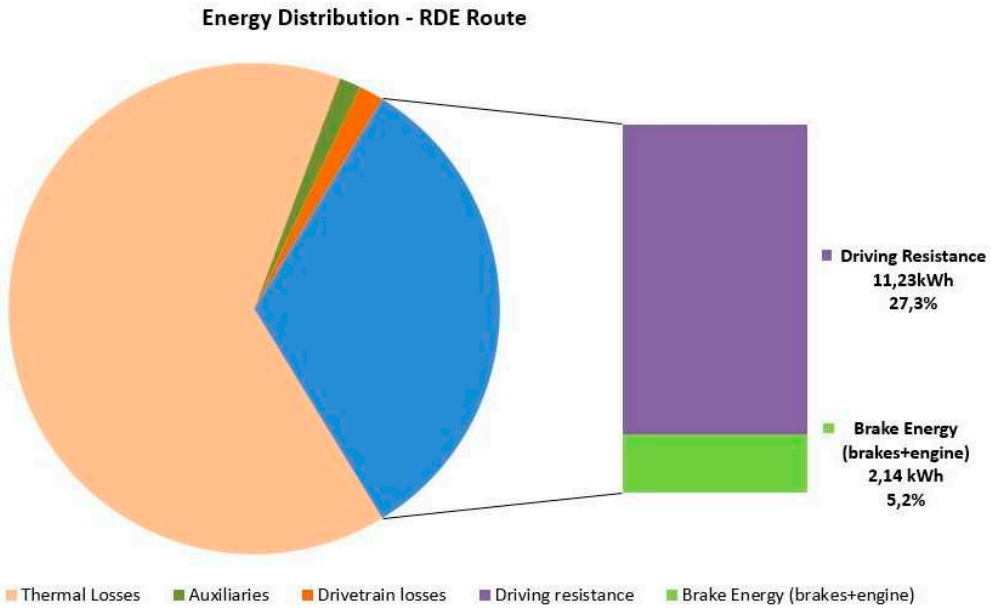

Figure 7. Vehicle energy balance.

The overall efficiency of the internal combustion engine in the test conditions of the vehicle was quite high, over 32%, but it should be emphasized that the efficiency in city driving conditions is far lower and in certain conditions falls below 10%, while the maximum engine efficiency is around 42 %. This difference shows the utility of the hybrid drive, which has the ability to move the load point towards the higher efficiency. Of the total traction energy, 84% was spent on overcoming the vehicle's resistances and that part of energy is irreversible, while the rest was spent on vehicle braking and that can be returned to the system through regenerative braking. The testing was caried out on roads without a significant change in altitude and in conditions of moderate traffic, which resulted in more

Preprints (www.preprints.org) | NOT PEER-REVIEWED | Posted: 9 November 2023 doi:10.20944/preprints202311.0600.v1

uniform driving with only 16% reversible energy. The distribution of emissions and traction energy according to power classes is shown in a bar graph in Figure 6, where all energy values are shown relative to the total positive traction energy of the RDE cycle, while emissions are shown as a percentage of the total emissions generated during the cycle. The relevant parameters for the comparison of the VSP non-hybrid model and CruiseM non-hybrid vehicle model are presented in Table 3.

Table 3. The relevant parameters for the comparison of the VSP and CruiseM models.

Clasic vehicle	**RDE cycle**			**RDE [1/km]**			**Deviation**			
	Measured	CruiseM	VSP	Measured	CruiseM	VSP	CruiseM	CruiseM [%]	VSP	VSP [%]
Distance [km]	86.21	86.63	86.21	1.000	1.005	1.000	0.005	0.48%	0.000	0.00%
Positive Traction energy [kWh]	13.37	13.33	13.46	0.155	0.154	0.156	-0.035	0.22%	0.092	0.69%
Negative Trac. energy [kWh]	-2.14	-2.22	-2.27	-0.0248	-0.0256	-0.0263	-0.080	3.26%	-0.130	6.08%
CO_2 emission [g]	10540	10556	10540	122.2	121.9	122.2	16.259	-0.33%	0.000	0.00%
NOx emission [mg]	39806	40051	39806	461.7	462.3	461.7	245.136	0.13%	0.000	0.00%
Consumption [kg]	3.366	3.371	3.366	0.039	0.039	0.039	0.005	-0.33%	0.000	0.00%

The distance and emissions of the VSP non-hybrid model match the measured data perfectly because the model was calculated using those parameters. Positive and negative traction energy deviate from the measured values because they are calculated via Equation (2) based on current specific power. The distance deviation of the CruiseM model is a consequence of Forward approach which controls velocity using PI regulator. In this approach the driving cycle is not perfectly followed because it considers system response time. Deviations of positive traction energy, distance, consumption and CO_2 emissions are within 1% of actual values. Only the relative negative traction energy significantly deviates between the two models, while the absolute deviation is small due to the small value of negative traction energy. The reason for this deviation is the same as for the distance deviation.

3.2. Testing of Hybrid and VSP Vehicle Models in RDE, NEDC and WLTC Driving Cycles

Both hybrid models were tested and compared using standard cycles, the RDE cycle which is identical to the already performed measurement, the NEDC cycle which is outdated by today's standards and in the WLTC cycle which has gradually replaced NEDC. The CruiseM model is optimized based on set of simple rules described with global objective function. The VSP model works in the frequency domain, so it does not have the possibility of real-time optimization, but the same rules can be used to compare these two models. In this case, the primary goal is to compare the two models so that the VSP frequency model follows the conditions of the CruiseM model. The objective function is minimization of CO_2 emissions or consumption, so the optimization prefers medium and higher power classes in which the internal combustion engine works more efficiently. On the other hand, the highest classes generate high NOx emissions, which in this case are not penalized because they are not covered by the objective function (14). The distribution of traction energy, emissions, and consumption for the hybrid vehicle under the RDE cycle is graphically depicted in Figure 8A using a bar chart.

Preprints (www.preprints.org) | NOT PEER-REVIEWED | Posted: 9 November 2023 doi:10.20944/preprints202311.0600.v1

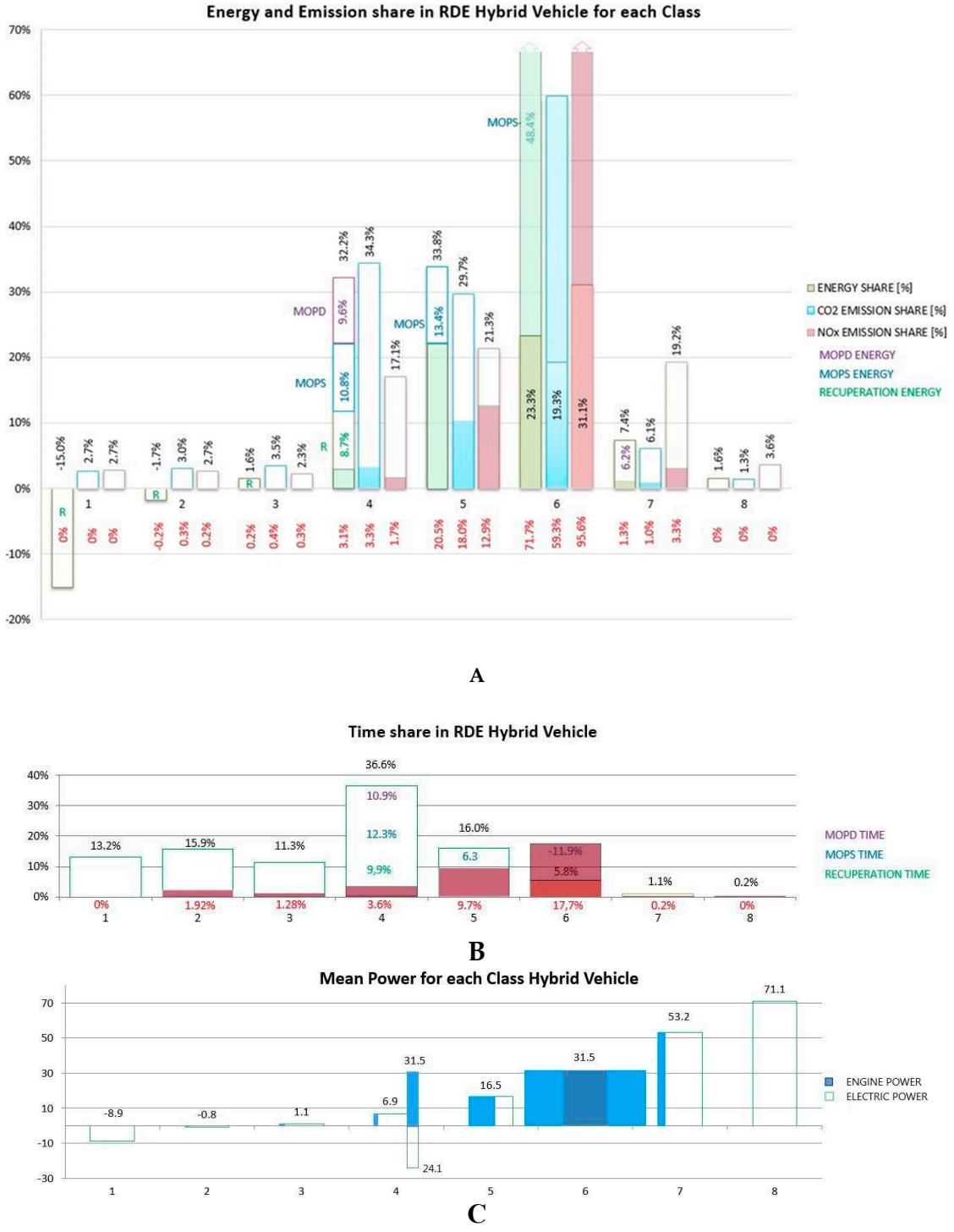

Figure 8. A. Energy distribution and emissions of the VSP hybrid model in the RDE cycle. **B.** Time shares of power classes.**C.** Time shares of power classes.

All emissions and energy shares are expressed relative to the emissions of a non-hybrid vehicle and to the positive traction energy of each cycle respectively. Classes 1 and 2 have a negative traction power where any engine operation is generally unnecessary, but regenerative braking is possible. The internal combustion engine remains switched on in class 2 only 1.92% of the time, Figure 8B, consuming 0.2% of the total traction energy, Figure 8A. This small amount of energy consumption is not the most optimal solution from an energy point of view, but it is a consequence of replicating the energy management strategy of the CruiseM model.

Preprints (www.preprints.org) | NOT PEER-REVIEWED | Posted: 9 November 2023 doi:10.20944/preprints202311.0600.v1

Class 3 represents the lowest values of positive traction power with a mean power of 1.1kW, Figure 8C. This engine operating region is very inefficient, so the goal is to completely eliminate the engine's work and replace that energy with stored regenerative braking energy. The engine remained in operation for only 1.28% compared to 11.3% of the total operation time of the non-hybrid vehicle, Figure 8B and generated 0.2% of the total traction energy, Figure 8A, the same as in the CruiseM model. In class 3, the vehicle emits 0.4% instead of the initial 3.5% of CO_2 emissions and 0.3% of NOx emissions instead of the initial 2.3%.

Class 4 has a slightly higher average power of 6.9kW, but still deep in the inefficient region in terms of consumption and CO_2 emissions. With a hybrid drive, it would be desirable to completely eliminate the operation of the engine in this region as well, but the engine remains on for 3.6% of the total driving time, Figure 8B generating 3.1% of the total traction energy. Class 4 contains 32.2% of the total traction energy, where 8.7% of energy was gained from regenerative braking. The remaining 20.4% was obtained by moving the operating region of the engine to a more efficient class 6. Of the 20.4% of the mentioned energy, 9.6% was obtained directly from the internal combustion engine operating in a higher class and this is marked in Figure 8A as Moving Operating Point Direct (MOPD), while 10.8% is obtained from stored energy from the battery, which is generated as excess engine energy gained from moving engine operating point, marked on the graph as Moving Operating Point Stored (MOPS). Considering the time shares of individual classes, Figure 8C, the engine works only 3.6% of the time with the power of the original class, 10.9% of the time it works with the average power of the preferred 6th class, and in the remaining time the vehicle is powered by energy from the battery, 9.9% from regenerative braking and 12.3% from MOPS. In class 4, the vehicle emits 3.3% instead of the initial 34.3% of CO_2 emissions and 1.7% of NOx emissions instead of the initial 17.1%.

In class 5, 20.5% of the energy comes from the internal combustion engine, while the rest of 13.4% is used from the battery and gained through MOPS. The engine generates 18% of CO_2 emissions instead of the initial 29.7% and 12.9% of NOx emissions instead of the initial 21.3%. Class 6 is the preferred considering engine efficiency, so the share of internal combustion engine energy increases in favor of other classes from 23.3% to 71.7% of the total initial traction energy. At the same time, CO_2 emissions of class 6 increase from 19.3% to 29.3% of initial total CO_2 emissions, while NOx emissions increase from 31.1% to 95.6%.

Class 7 also belongs to the less efficient region, compared to class 6, and engine energy covers only 1.3% of the initial required 7.4%. This 1.3% of the traction energy also results from the CruiseM model energy management strategy. The total CO_2 emissions of the hybrid vehicle were reduced from 6.1% to 1%, while NOx emissions were reduced from 19.2% to 3.3%. The bar diagram in Figure 10 shows the comparative results of the vehicle travelled distance for VSP and CruiseM models of hybrid and non-hybrid vehicles in RDE, NEDC and WLTP cycles. In contrast to Table 3, where the deviations were expressed in relation to the measured values of the RDE cycle, the following bar diagrams show the deviations between the VSP and CruiseM models.

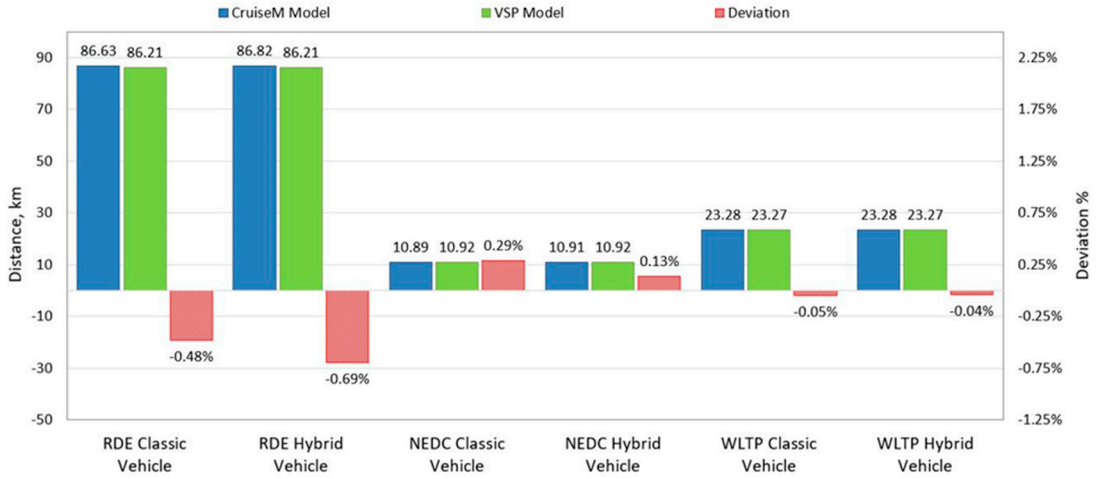

Preprints (www.preprints.org) | NOT PEER-REVIEWED | Posted: 9 November 2023 doi:10.20944/preprints202311.0600.v1

Figure 9. Comparison of distances covered for different models and cycles.

As before mentioned, the cause of the deviation between the two models lies in different modeling approaches, the VSP was created as a backward model that perfectly follows the given speed profile, while the deviation of the travelled distance of the CruiseM model is a consequence of the forward approach which includes the PI regulator in this case. Despite different approaches, the maximum deviation of the travelled distance is less than 0.7%, which is a more than acceptable result. In the RDE cycle, the travelled distance of both models deviates the most, -0.69% for the hybrid model, and -0.48% for the non-hybrid model. Better results were achieved with laboratory cycles compared to the RDE cycle. One of the important reasons is certainly the influence of altitude, which laboratory cycles do not have. In the NEDC cycle, the travelled distance of classic vehicles differs by 0.29% for a non-hybrid vehicle and 0.13% for a hybrid vehicle. The smallest deviations of 0.05% for the non-hybrid vehicle and 0.04% for the hybrid vehicle were recorded in the WLTP cycle. Although the deviations in the travelled distance are small, they were taken into account as a corrective factor when comparing other parameters. The bar graphs in Figures 10 and 11 show the comparative results of positive and negative traction energies required for the vehicle to overcome the test driving cycles for different cycles. The differences that arise in the traction energies are also a consequence of the forward model, i.e. the settings of the PI regulator. The largest deviation of positive traction energy was recorded between RDE models of hybrid vehicles at 2.85%. Relative deviations of negative traction energies are significantly higher due to small absolute amounts, but the absolute amounts are small and acceptable considering the impact on emissions and consumption. The largest relative deviation of negative traction energies is shown by the non-hybrid vehicle model in the WLTP cycle of over 8%, but on an absolute scale only 0.07kWh.

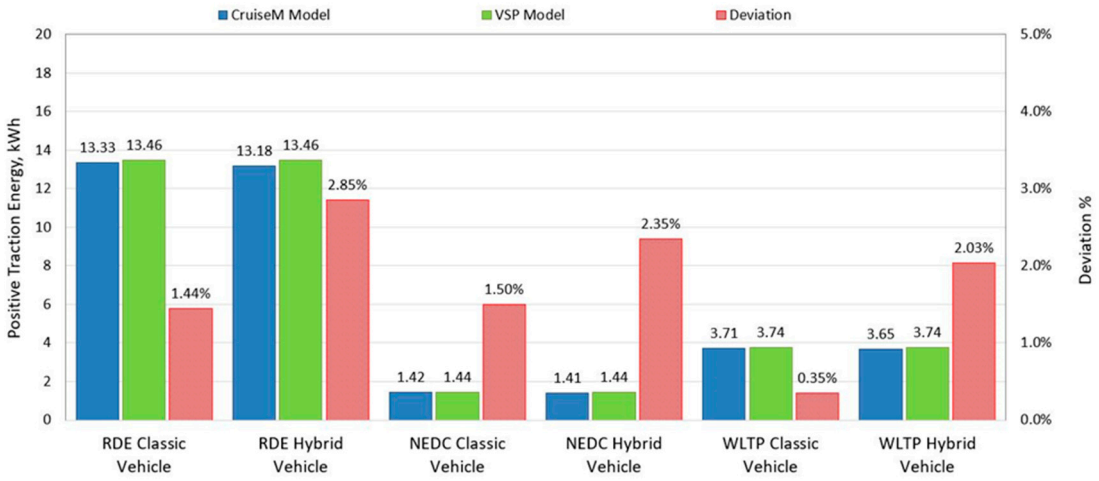

Figure 10. Comparison of positive traction energies for different models and cycles.

Preprints (www.preprints.org) | NOT PEER-REVIEWED | Posted: 9 November 2023 doi:10.20944/preprints202311.0600.v1

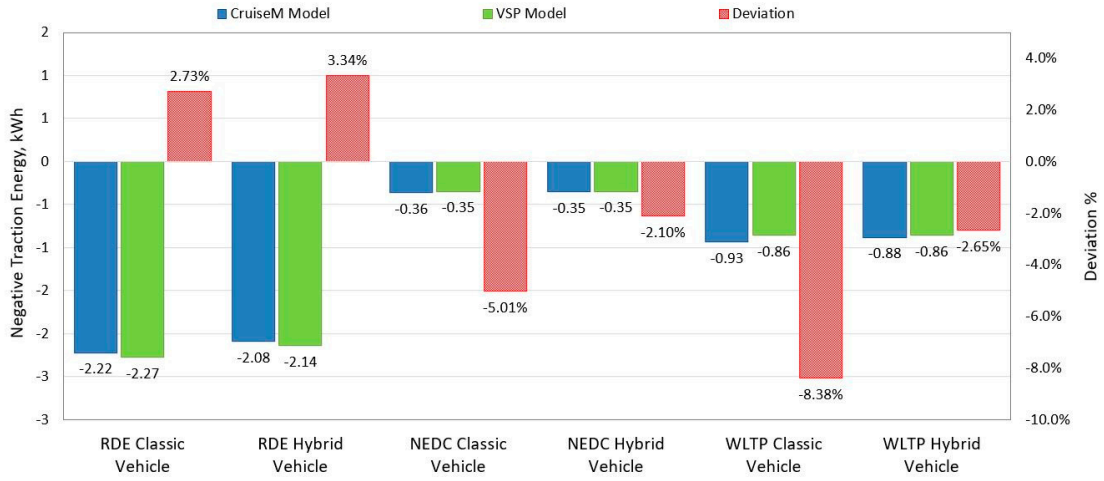

Figure 11. Comparison of negative traction energies for different models and cycles.

The comparison of CO_2 emissions and fuel consumption is shown in the bar diagrams in Figures 12 and 13. CO_2 emissions are expressed in absolute values i.e., in grams and corrected according to the travelled distance, while consumption is traditionally expressed in litres per 100 kilometres. The most significant deviations were recorded for the hybrid vehicle model in RDE conditions at 3.79% and for the non-hybrid vehicle model in the WLTP cycle at 4.4%. If we compare the results according to cycles, the NEDC cycle in both modelled vehicles, hybrid and classic, gives deviations slightly higher than 1%. The CruiseM model was used as a reference, but it is possible that this model also causes some deviations because it does not include transients.

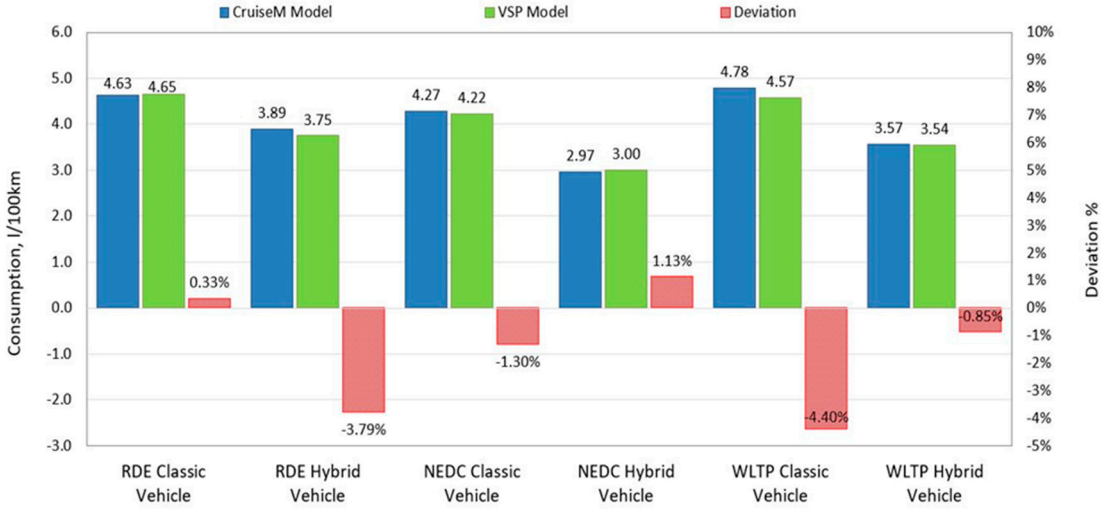

Figure 12. Comparison of consumption per 100 km for different models and cycles.

Preprints (www.preprints.org) | NOT PEER-REVIEWED | Posted: 9 November 2023 doi:10.20944/preprints202311.0600.v1

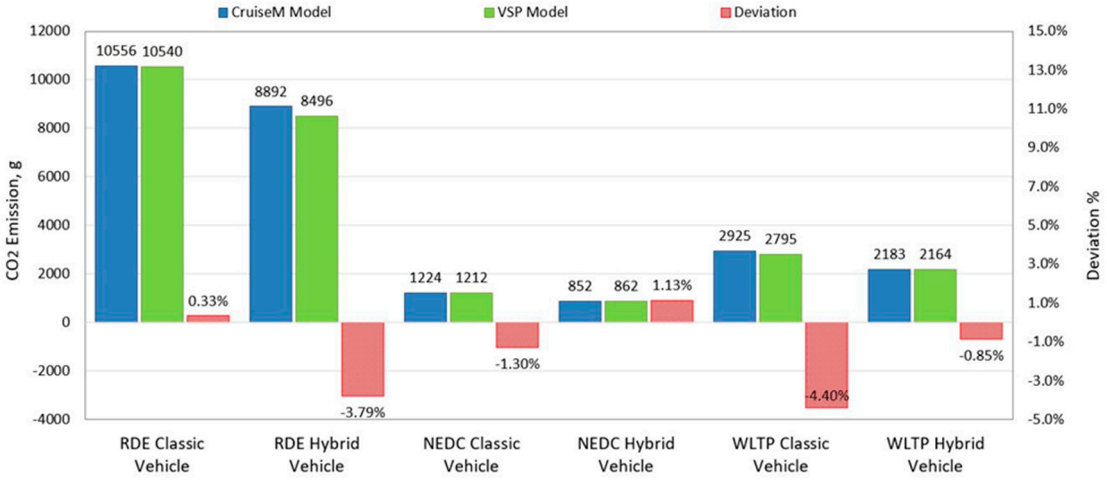

Figure 13. Comparison of CO_2 emissions for different models and cycles.

The reason for the good overlap between the results of the NEDC cycle lies in the cycle itself, with constant accelerations where the classic CruiseM model which is based on consumption and emission maps approximates the real situation relatively well due to less influence of transient phenomena.

Since the vehicle is type approved according to the Euro 6b standard, which includes testing in laboratory conditions according to the NEDC cycle, it is possible to compare the results with the type approved values. The declared value of CO_2 emissions in the NEDC cycle for the tested vehicle is 102 g/km, while the value of CO_2 emissions of the modelled vehicle is slightly less than 111 g/km. A deviation of 8.8% was expected considering that the type approval procedure at that time was performed on the "golden vehicle" which gave significantly better results than the tested one. All these results of the hybrid models were achieved by following a strategy of the CruiseM model based on set of rules, but the best result achieved by optimizing the VSP hybrid model, without taking into account the CruiseM strategy, in terms of CO_2 emissions gives about 4% better results than those shown in Figure 13, which would put this vehicle inside legal limit of 95g of CO_2 emissions in real conditions.

The absolute amounts and corrected deviations of NOx emissions of both models applied to different cycles are shown by a bar graph in Figure 14. The deviations of NOx emissions are on average slightly higher than CO_2 emissions and fuel consumption primarily due to the larger possible deviations of the classic map-based CruiseM model that does not include transients. Transient phenomena in the assessment of NOx emissions have a greater impact due to the way NOx emissions are regulated through exhaust gas recirculation [8].

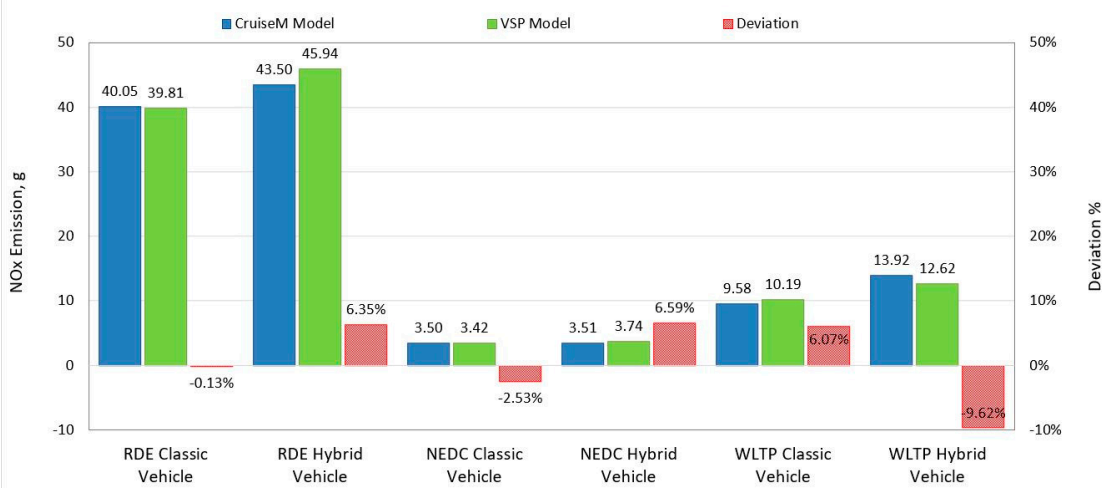

Figure 14. Comparison of NOx emissions for different models and cycles.

 doi:10.20944/preprints202311.0600.v1

The largest deviations of NOx emissions of 9.62% are shown with the hybrid vehicle models in the WLTP cycle, while the same models in the NEDC and RDE cycles show deviations slightly higher than 6%. Non-hybrid vehicle models in RDE, NEDC and WLTP conditions differ by 0.13%, 2.53% and 6.07%, respectively. Larger deviations in the WLTP cycle, especially in NOx emissions, are expected due to extremely dynamic driving.

4. Conclusions

The paper presents a VSP model based on frequency analysis, which represents a new way of modeling primarily hybrid, but also classic non-hybrid vehicles. A comparison of two independent models, VSP and CruiseM, was performed in order to prove the usefulness of the much simpler VSP model with the possibility of obtaining results with similar accuracy. Positive and negative traction energies data, which are necessary to follow the desired cycle, as well as CO_2 emissions data, fuel consumption and NOx emissions, were analyzed and compared. First, the VSP model was tested on a hybrid vehicle under RDE conditions following the same rule-based strategy as the CruiseM model. Furthermore, the energy balance calculation is presented in detail, as well as the calculation of the corresponding CO_2 and NOx emissions for each individual class. All hybrid modes time shares, as well as the shares of individual traction energy components and average ICE power are graphically presented and classified into the necessary traction power classes. Absolute comparative data are presented graphically with all deviations expressed relatively with a correction according to the travelled distances. The deviations of the travelled distances are very low with the highest value of 0.69% for the hybrid vehicle and the RDE cycle. The causes of the deviations lie in the different modeling approaches, Backward approach for the VSP model and Forward approach for the CruiseM model, where PI controller causes slight deviations. All positive traction energies have positive deviations of the VSP model between 0.35% for the WLTP model of the non-hybrid vehicle to a maximum of 2.85% for the RDE hybrid model. The deviations of the negative traction energy are relatively higher, up to 8.38%, which is expected because of their small absolute values compared to the total positive traction energy, so they have negligible impact to the overall results. The most important element of the comparison of the two models are CO_2 emissions and fuel consumption, where the biggest deviation of the results was recorded for the hybrid model of the vehicle in RDE cycle conditions of 3.79% and for the non-hybrid vehicle model in WLTP conditions of 4.4%. All other combinations of cycles and models give deviations of about 1%, which is an excellent result that directly proves the reliability of the model. The best result obtained by optimizing the VSP model of the hybrid vehicle in RDE conditions, independently of CruiseM model, is about 4% better relative to the result obtained following the CruiseM strategy. This outcome means that this vehicle would reach the legally prescribed, penalty-free limit of 95g/km under real-world conditions. Regarding the results of the comparison of NOx emissions, the deviations are somewhat larger compared to CO_2 emissions and consumption. The largest deviations of NOx emissions of 9.62% are shown by the hybrid vehicle models in the WLTP cycle, while the same models in the NEDC and RDE cycles show deviations slightly higher than 6%. Models of non-hybrid vehicles in RDE, NEDC and WLTP conditions differ by 0.13%, 2.53% and 6.07%, respectively. Larger deviations of these emissions are expected due to the worse performance of the CruiseM model in predicting NOx emissions which are controlled by the EGR system, which is very sensitive to transient phenomena that are not described by this model. This research showed very good results of the simpler VSP model in predicting fuel consumption and CO_2 and NOx emissions without using complex time domain models which require great skills and complex algorithms to realize real objective functions. Another problem of the time domain model is that it sometimes gets stuck in local minima without finding an optimal global solution, so there is also the possibility of using the VSP model as a control mechanism of the time domain model. Such a model enables a much simpler definition of the objective function, and thus the simplification of the optimization of complex energy management systems such as hybrid propulsion systems. Future research should be directed towards determining the influence of various parameters of the VSP model on its accuracy, especially the selection of the number of classes

and their ranges. The possibility of expanding the model in a multidimensional domain should also be investigated, that is, it should be expanded with additional influential parameters.

Author Contributions: Conceptualization, A.K.; methodology, A.K.; software, A.K., T.V., A.V.; validation, A.K., T.V., A.V.; formal analysis, A.K., T.V., G.R., A.V.; investigation, A.K., T.V., G.R.; resources, A.K., T.V., G.R., A.V.; data curation, A.K., T.V.; original draft preparation, A.K.; writing, A.K., T.V., G.R .; visualization, A.K..; supervision, G.R.; project administration, G.R.; funding acquisition, G.R.. All authors have read and agreed to the published version of the manuscript.

Funding: This work has been fully supported by the Croatian Science Foundation under the project IP.2020-02-6249.

Data Availability Statement: The data used in this study are reported in the paper figures and tables.

Acknowledgments: The authors would like to thank Faculty of Mechanical Engineering and Naval Architecture from Zagreb for contribution in experimental research and AVL, Graz for software support.

Conflicts of Interest: The authors declare no conflict of interest.

References

1. E. P. News. "EU Ban on the Sale of New Petrol and Diesel Cars from 2035 Explained." https://www.europarl.europa.eu/news/en/headlines/economy/20221019STO44572/eu-ban-on-sale-of-new-petrol-and-diesel-cars-from-2035-explained (accessed 26. August 2023).
2. B. Mali, A. Shrestha, A. Chapagain, R. Bishwokarma, P. Kumar, and F. Gonzalez-Longatt, "Challenges in the penetration of electric vehicles in developing countries with a focus on Nepal," *Renewable Energy Focus,* vol. 40, pp. 1-12, 2022.
3. M. A. Ktistakis, J. Pavlovic, and G. Fontaras, "Sampling approaches for road vehicle fuel consumption monitoring," *Report EUR,* vol. 30420, 2021.
4. (2019). *Regulation (EU) 2019/631 of the European Parliament and of the Council of 17 April 2019 setting CO2 emission performance standards for new passenger cars and for new light commercial vehicles, and repealing Regulations (EC) No 443/2009 and (EU) No 510/2011*. [Online] Available: http://data.europa.eu/eli/reg/2019/631/oj
5. T. Takaishi, A. Numata, R. Nakano, and K. Sakaguchi, "Approach to High Efficiency Diesel and Gas Engines," 2008.
6. I. Pielecha, W. Cieślik, and A. Szałek, "Energy recovery potential through regenerative braking for a hybrid electric vehicle in a urban conditions," in *IOP Conference Series: Earth and Environmental Science*, 2019, vol. 214, no. 1: IOP Publishing, p. 012013.
7. "Driving into 2025: The Future of Electric Vehicles." J.P. Morgan. (accessed 25 May, 2022).
8. A. Kozina, G. Radica, and S. Nižetić, "Analysis of methods towards reduction of harmful pollutants from diesel engines," *Journal of Cleaner Production,* vol. 262, p. 121105, 2020.
9. S. Reshma, E. R. Samuel, and A. Unnikrishnan, "A Review of various internal combustion engine and electric propulsion in hybrid electric vehicles," in *2019 2nd International Conference on Intelligent Computing, Instrumentation and Control Technologies (ICICICT)*, 2019, vol. 1: IEEE, pp. 316-321.
10. S. S. Ravi, J. Mazumder, J. Sun, C. Brace, and J. W. Turner, "Techno-Economic assessment of synthetic E-Fuels derived from atmospheric CO2 and green hydrogen," *Energy Conversion and Management,* vol. 291, p. 117271, 2023.
11. A. Vučetić *et al.*, "Real Driving Emission from Vehicle Fuelled by Petrol and Liquefied Petroleum Gas (LPG)," *Cognitive Sustainability,* vol. 1, no. 4, 2022.
12. U. K. Medževeprytė, R. Makaras, V. Lukoševičius, and S. Kilikevičius, "Application and Efficiency of a Series-Hybrid Drive for Agricultural Use Based on a Modified Version of the World Harmonized Transient Cycle," *Energies,* vol. 16, no. 14, p. 5379, 2023.
13. S. Schulze, G. Feyerl, and S. Pischinger, "Advanced ECMS for hybrid electric heavy-duty trucks with predictive battery discharge and adaptive operating strategy under real driving conditions," *Energies,* vol. 16, no. 13, p. 5171, 2023.
14. A. Kampker, C. Offermanns, H. Heimes, and P. Bi, "Meta-analysis on the Market Development of Electrified Vehicles," *ATZ worldwide,* vol. 123, no. 7, pp. 58-63, 2021.
15. M. Sabri, K. A. Danapalasingam, and M. F. Rahmat, "A review on hybrid electric vehicles architecture and energy management strategies," *Renewable and Sustainable Energy Reviews,* vol. 53, pp. 1433-1442, 2016.
16. K. Ç. Bayindir, M. A. Gözüküçük, and A. Teke, "A comprehensive overview of hybrid electric vehicle: Powertrain configurations, powertrain control techniques and electronic control units," *Energy conversion and Management,* vol. 52, no. 2, pp. 1305-1313, 2011.
17. P. Zhang, F. Yan, and C. Du, "A comprehensive analysis of energy management strategies for hybrid electric vehicles based on bibliometrics," *Renewable and Sustainable Energy Reviews,* vol. 48, pp. 88-104, 2015.

18. F. R. Salmasi, "Control strategies for hybrid electric vehicles: Evolution, classification, comparison, and future trends," *IEEE Transactions on vehicular technology,* vol. 56, no. 5, pp. 2393-2404, 2007.
19. A. M. Ali and D. Söffker, "Towards optimal power management of hybrid electric vehicles in real-time: A review on methods, challenges, and state-of-the-art solutions," *Energies,* vol. 11, no. 3, p. 476, 2018.
20. W. Liu, *Introduction to hybrid vehicle system modeling and control*. John Wiley & Sons, 2013.
21. W. Enang and C. Bannister, "Modelling and control of hybrid electric vehicles (A comprehensive review)," *Renewable and Sustainable Energy Reviews,* vol. 74, pp. 1210-1239, 2017.
22. C. C. Chan, A. Bouscayrol, and K. Chen, "Electric, hybrid, and fuel-cell vehicles: Architectures and modeling," *IEEE transactions on vehicular technology,* vol. 59, no. 2, pp. 589-598, 2009.
23. S. Onori, L. Serrao, and G. Rizzoni, "Hybrid electric vehicles: Energy management strategies," 2016.
24. D.-D. Tran, M. Vafaeipour, M. El Baghdadi, R. Barrero, J. Van Mierlo, and O. Hegazy, "Thorough state-of-the-art analysis of electric and hybrid vehicle powertrains: Topologies and integrated energy management strategies," *Renewable and Sustainable Energy Reviews,* vol. 119, p. 109596, 2020.
25. I. Preda, D. Covaciu, and G. Ciolan, "Coast down test–theoretical and experimental approach," 2010.
26. F. Zhang, L. Wang, S. Coskun, H. Pang, Y. Cui, and J. Xi, "Energy management strategies for hybrid electric vehicles: Review, classification, comparison, and outlook," *Energies,* vol. 13, no. 13, p. 3352, 2020.
27. J. L. Jimenez-Palacios, "Understanding and quantifying motor vehicle emissions with vehicle specific power and TILDAS remote sensing," *Massachusetts Institute of Technology,* 1998.
28. J. Lee and D. J. Nelson, "Rotating inertia impact on propulsion and regenerative braking for electric motor driven vehicles," in *2005 IEEE Vehicle Power and Propulsion Conference*, 2005: IEEE, p. 7 pp.
29. (2016). *COMMISSION REGULATION (EU) 2016/427; amending Regulation (EC) No 692/2008 as regards emissions from light passenger and commercial vehicles (Euro 6)*.
30. A. Kozina, G. Radica, and S. Nižetić, "Hybrid Vehicles Emissions Assessment," in *2021 6th International Conference on Smart and Sustainable Technologies (SpliTech)*, 2021: IEEE, pp. 1-5.